ACS APPLIED MATERIALS & INTERFACES

Research Article

Cite This: ACS Appl. Mater. Interfaces 2018, 10, 5933−5940

www.acsami.org

Halloysite Nanotube-Modified Plasmonic Interface for Highly Sensitive Refractive Index Sensing

Mei Yang,[†] Xin Xiong,[†] Rui He,[‡] Yunhan Luo,[*,†,§] Jieyuan Tang,[§,∥] Jiangli Dong,[§,∥] Huihui Lu,[†,∥] Jianhui Yu,[†,∥] Heyuan Guan,[†,§] Jun Zhang,[∥] Zhe Chen,[§,∥] and Mingxian Liu[*,‡]

[†]Guangdong Provincial Key Laboratory of Optical Fiber Sensing and Communications, [‡]Department of Materials Science and Engineering, [§]Key Laboratory of Optoelectronic Information and Sensing Technologies of Guangdong Higher Education Institutes, and [∥]Key Laboratory of Visible Light Communications of Guangzhou, Jinan University, Guangzhou 510632, China

Supporting Information

ABSTRACT: We propose and demonstrate a novel strategy to modify the plasmonic interface by using a thin layer of halloysite nanotubes (HNTs). The modified surface plasmon resonance (SPR) sensor achieves a greatly improved sensitivity because the large surface area and high refractive index of the HNTs layer significantly increase the probing electric field intensity and hence the measurement sensitivity. More significantly, the thickness of the HNTs layer can be tailored by spraying different concentrations of HNTs ethanol suspension. The proposed sensors show significant superiority in terms of the highest sensitivity (10431 nm/RIU) and the enhancement fold (5.6-folds) over those reported previously. Additionally, the proposed approach is a chemical-free and environment-friendly modification method for the sensor interface, without additional chemical or biological amplification steps (no toxic solvents are used). These unique features make the proposed HNTs-SPR biosensor a simple, biocompatible, and low-cost platform for the trace-level detection of biochemical species in a rapid, sensitive, and nondestructive manner.

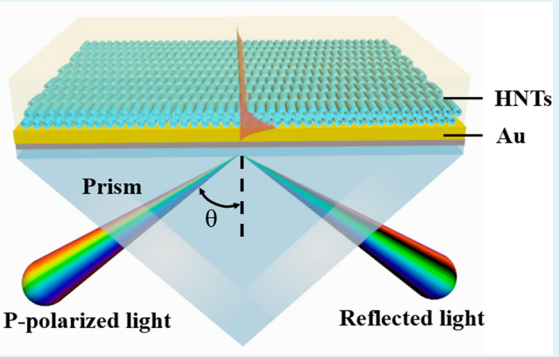

KEYWORDS: *surface plasmon resonance, interface, halloysite nanotubes, sensitivity, refractive index*

INTRODUCTION

Surface plasmon resonance (SPR) is a sensitive optical technique for biochemical detection via monitoring the changes of the refractive index (RI) of the surrounding medium of the metallic interface due to its strong evanescent field.[1,2] In recent years, SPR sensors have attracted great attention as one of the leading optical sensing technologies because of their inherent advantages such as real-time operation, label-free analysis, and high sensitivity.[3−8] However, the use of SPR sensors is currently limited in the direct detection of small molecules, at ultralow concentration of analytes, and in low-affinity interactions.[9−11] To extend their usage, various methods have been proposed to modify the plasmonic interface and hence to improve their sensitivity, most of which are based on nanomaterials such as metallic nanoparticles,[12,13] magnetic nanoparticles,[14] carbon-based nanostructures,[15] latex nanoparticles, and liposome nanoparticles.[12] It is worth noting that the effect of the nanoparticle-modified interface to amplify the SPR signal can be categorized as follows: (i) increasing the probing electric field;[16,17] (ii) increasing the surface area;[12,18] and (iii) the combined effect from (i) and (ii).[19]

The probing electric field near the metallic interface can be increased by evaporating a nanomaterial layer with a relatively higher RI than the matrix onto the top of the metallic thin film.[20−23] The added high-RI nanomaterials include TiO_2, ZnO, and silicon, which can induce a larger evanescent field and thereby increase the probing sensitivity. Alternatively, the probing electric field can be increased by introducing noble metallic nanoparticles to couple the localized SPR to the propagating SPR.[24−27] The greatly amplified local electric field around the nanoparticles and their large surface area can enhance the sensing ability. However, the success of this enhancement depends largely on the material, structure, and size of the nanoparticles.[17,19] The challenge of synthesizing and size controlling of such nanoparticles has limited their applications. It has been recently demonstrated that SPR sensors decorated by two-dimensional materials, such as graphene and tungsten disulfide (WS_2), could achieve a sensitivity enhancement.[28−32] This is probably due to the larger surface area of these materials and the strong excited electric field enhancement because the high mobility of carriers provided by both graphene and WS_2 has led to a high charge transfer between the decorated material and the metallic thin film, thus increasing the probing electric field. Unfortunately, the inherent absorption of these materials in the visible range will broaden the SPR dip, and the decoration suffers from complicate and expensive synthesis procedures such as chemical vapor deposition. An ideal candidate nanomaterial desired for modifying the plasmonic interface will integrate the

Received: October 30, 2017
Accepted: January 17, 2018
Published: February 2, 2018

DOI: 10.1021/acsami.7b16511
ACS Appl. Mater. Interfaces 2018, 10, 5933−5940

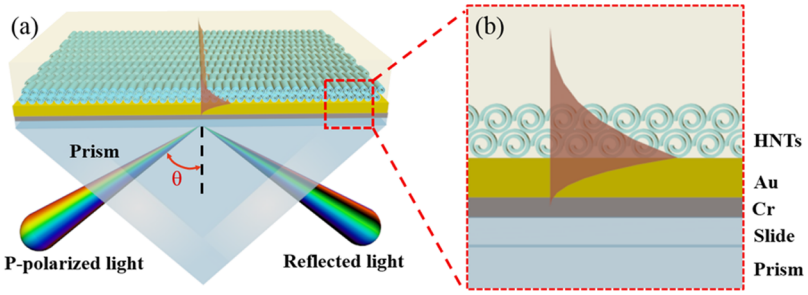

Figure 1. (a) Three-dimensional model of the structure of the proposed HNTs-SPR sensor; (b) enlarged view of the region marked by the square in (a).

merits mentioned above, namely, high RI, large surface area, and strong charge transfer to the metallic substrate film. Meanwhile, some other features such as easy to synthesis or abundance and its capability to boost the sensitivity are also of vital importance.

Halloysite nanotubes (HNTs), derived from natural mineral deposits, represent a novel nanomaterial for various sensor applications because of their excellent interface properties. Chemically, HNTs are similar to kaolin with a formula of $Al_2(OH)_4Si_2O_5{\cdot}nH_2O$. HNTs have a distinctive morphology of a hollow cylinder with inner diameter, outer diameter, and length in the range of 10−20, 40−70, and 300−1500 nm, respectively.[33−35] Several studies have focused on the applications of HNTs as nanovectors for loading, storage, and controlled release of objects, such as drugs,[36] antibacterial,[37] and tumor cells.[38] The excellent performance of HNTs in various fields is largely due to their versatile properties, such as a high aspect ratio, high mechanical strength, high dispersion ability, good biocompatibility, thermal stability, low cost, and abundance.[24,39−41] For sensing applications, HNTs show a relatively high RI of 1.550,[42] which is a benefit for the enhancement of sensor sensitivity. In addition, the outer surface of HNTs is negatively charged by about −25 mV, which makes it easy to achieve a monodisperse state and leads to a strong charge transfer when they contact positive substance such as a metal substrate.[40] Recent studies have also illustrated the good biocompatibility of HNTs both in vitro and in vivo.[34,43] For example, HNTs can prompt wound healing and increase tumor cell capture ability.[40,44,45] Additionally, HNTs are proposed as supports to generate plasmonic platforms with remotely triggered heating capacity, by coating HNTs with gold nanoparticles.[46] Therefore, HNTs are expected to have good potential for sensing, especially for optical sensing, because of their large surface area, high RI, negatively charged surface, and good biocompatibility.

In this study, we propose a novel strategy to modify the SPR interface and demonstrate the SPR sensor with much improved sensitivity. On the basis of the Kretschmann attenuated total reflection structure, a 50 nm gold film is first coated on a 5 nm buffer layer of chromium (acting as an adhesive) before a uniform HNTs layer is sprayed. The HNTs-SPR sensor shows an extremely high sensitivity of 10 431 nm/RIU in the bulk solutions, which is 5.6-folds when compared to that of the conventional gold substrate. More importantly, the HNTs-SPR sensor shows even higher sensitivity enhancement fold in the bimolecular experiments than that in bulk solutions. To the best of our knowledge, this is the first demonstration utilizing HNTs for achieving higher measurement sensitivity in SPR sensors.

EXPERIMENTAL SECTION

Materials and Reagents. HNTs were purchased from Guangzhou Runwo Materials Technology Co., Ltd, China. Ethylene glycol, ethanol, phosphate buffer, and bovine serum albumin (BSA) solutions were purchased from Aladdin (Shanghai, China). HNTs ethanol suspensions with different concentrations were prepared by dispersing HNTs powder in anhydrous ethanol via ultrasonic treatment (Scientz-IID, Ningbo Xingzhi Biotechnology Co., Ltd, China) for 30 min. Aqueous solutions of ethylene glycol used to characterize the RI sensitivity of the sensor were prepared in laboratory, in which the RI was tested by Abbe refractometer (Edmund NT52-975, Edmund Optics Co., Ltd, China) at a room temperature of 25 °C.

Instruments. The absorbance of the HNTs ethanol suspension was determined using a spectrometer (AvaSpec-ULS2048XL, China) from 400 to 1100 nm. All SPR spectra were captured by the tungsten−halogen light source (AvaLight-HAL-(S)-Mini, China) with a wavelength ranging from 200 to 1160 nm and a spectrometer (AvaSpec-ULS2048XL, China) with the integrate time being 3.6 ms. The surface of SPR chips with and without HNTs coating was examined by a scanning electron microscopy (SEM) (Zeiss SteREO Discovery V20, Germany) SEM machine at 5 kV. Before SEM observation, a layer of gold was sputtered on the HNTs coating. The atomic force microscopy (AFM) observation of the different HNTs-SPR chips was performed using a Nanoscope IIIa controller (Veeco Instruments) in the tapping mode under ambient conditions at a scanning rate of 1 line/s. Ultrapure water from a Milli-Q water system was used to prepare the aqueous solutions.

Modification of HNTs-SPR Chip. The SPR chips were made from customized silica slides (Jiuyi Optics, Fuzhou, China). The slides were first cleaned by immersing into an ultrasonic machine for 10 min to remove any contaminants. A chromium adhesion layer (5 nm) and a gold film (50 nm) were deposited via vacuum evaporation. After being placed on a heating table of 80 °C for 2 min, the gold-coated slide surface was sprayed with the desired concentration of HNTs ethanol suspension for 10 s at a rate of 3 mL/s. To achieve a uniform HNTs coating, the cleaned gold-coated slides were fixed by tweezers, and the spray gun (Iwata, WA-101) was placed perpendicularly to the glass slides from a 7−10 cm distance and moved from top to bottom at a constant speed. The nozzle diameter was 1.0 mm, and spraying air pressure was 0.29 MPa at a flow rate of 3 mL/s. The spraying time was set as 10 s. The concentrations of the HNTs ethanol solution were 1, 2.5, 5, 7.5, and 10%. The sprayed HNTs layer acted as the medium for enhancing the sensitivity of the sensor. Each sensor was carefully cleaned by a soft brush and treated by an ultrasonic machine after measurement. The cleaned one was again sprayed with another concentration of HNTs suspension before being tested with the same procedure.

SPR Apparatus. The experimental apparatus, shown in Figure 1a, was a Kretschmann configuration SPR system whose cross section was depicted in Figure 1b. The HNTs-SPR chip was mounted on top of the prism with oil, which is applied for index matching. The SPR apparatus was operated in a wavelength modulation manner. Light from a tungsten−halogen light source was first polarized and then coupled into the prism. The evanescent light excited the surface plasmon of the gold film and formed a resonance dip in the reflected light, which was in turn recorded by a spectrometer.

DOI: 10.1021/acsami.7b16511
ACS Appl. Mater. Interfaces 2018, 10, 5933−5940

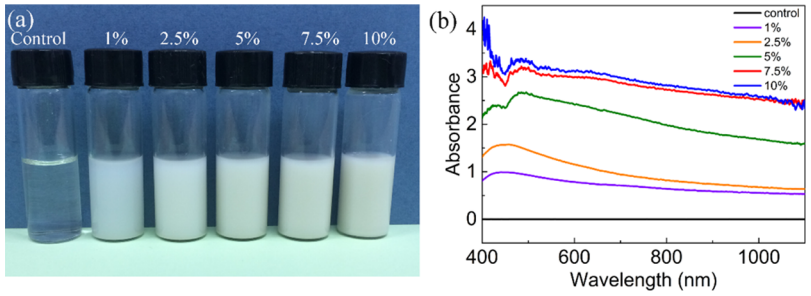

Figure 2. (a) Photographs of HNTs ethanol solutions with different concentrations; (b) absorption spectra of the prepared HNTs ethanol solutions.

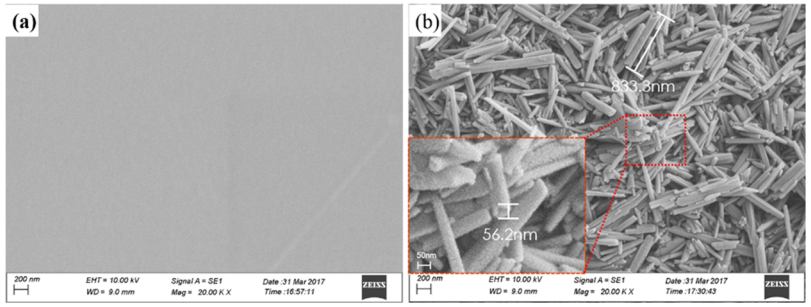

Figure 3. SEM photographs of (a) gold film and (b) prepared HNTs-SPR sensor surface.

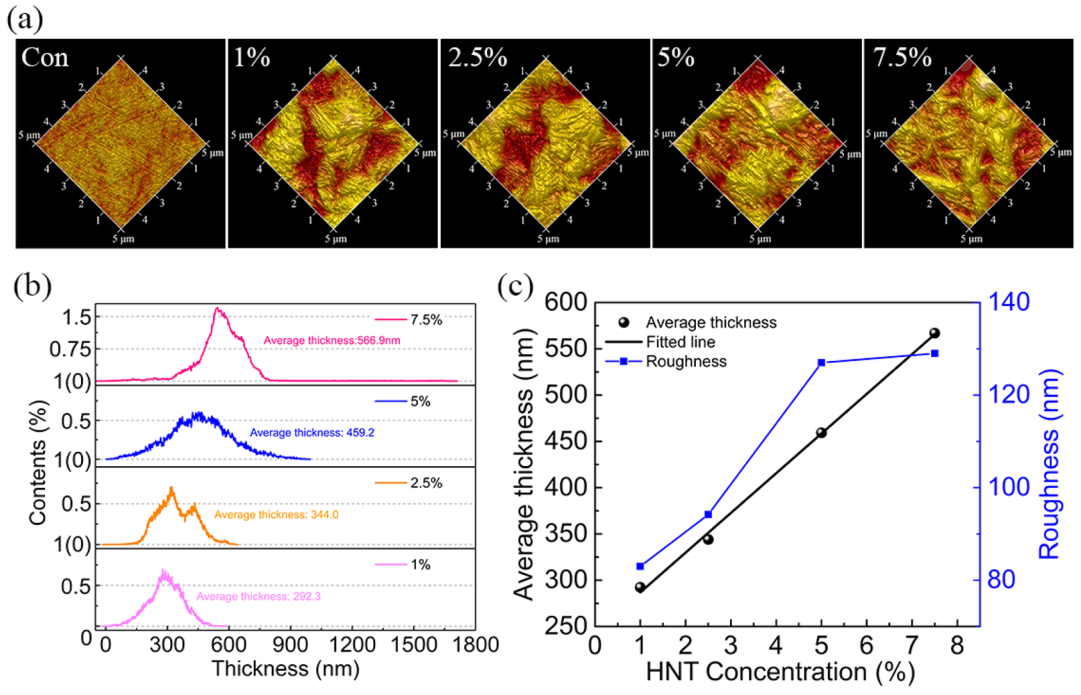

Figure 4. (a) Three-dimensional AFM image of different concentrations of the HNTs-SPR sensor surface; (b) line scanning height profile of HNTs coating with different concentrations; and (c) relationship between HNTs concentration and average thickness and roughness.

RESULTS AND DISCUSSION

Characterization of HNTs Coating. A good dispersion solution of HNTs in ethanol was achieved via ultrasonic treatment (Figure 2a). It was observed that the color of the dispersion solution transfers gradually from translucent to opaque with an increasing HNTs concentration. All dispersions are uniform and stable, which benefits for the following spray coating. The absorption spectra of the different dispersions were compared in Figure 2b. The spectrum of the ethanol sample was taken as a reference, whose absorbance curve was a straight line. The absorption spectra of HNTs suggest that there is no absorption band in the measured wavelength range from 400 to 1100 nm, whereas the extinctions increase with the HNTs concentration because of the increased scattering. A prior study found that there was a linear relationship between the absorbance value and the concentration of HNTs in aqueous dispersion.[47] The relatively flat absorption of HNTs excludes the interference from inherent absorption when the HNTs-SPR spectra were analyzed as follows.

DOI: 10.1021/acsami.7b16511
ACS Appl. Mater. Interfaces 2018, 10, 5933−5940

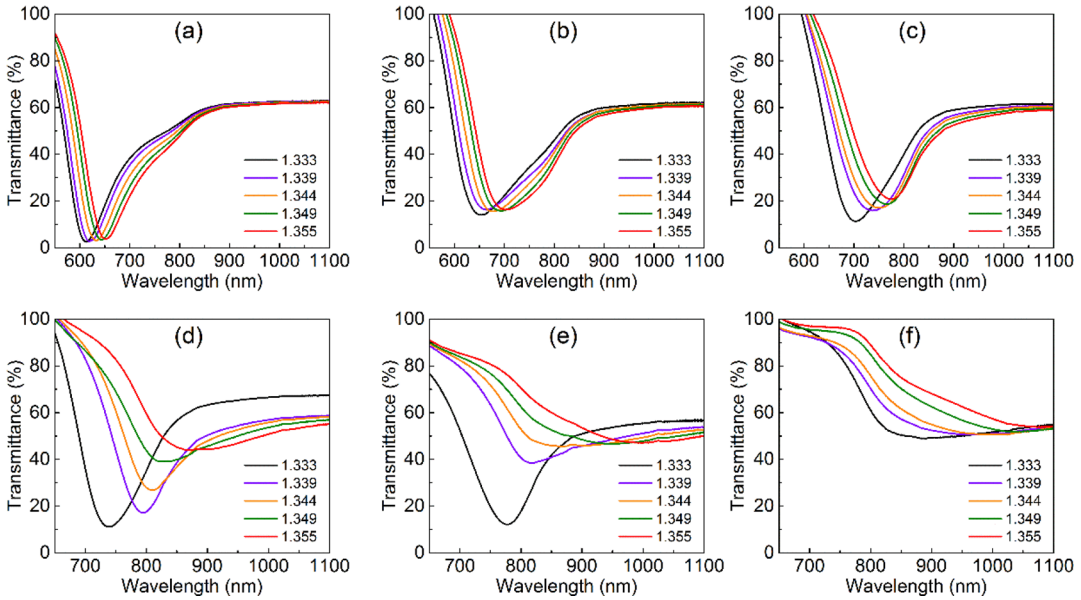

Figure 5. Transmittance spectra for the HNTs-SPR sensors coated with different HNTs solutions, with RI of the sensing medium changing from 1.333 to 1.355 RIU: (a) 0% HNTs; (b) 1% HNTs; (c) 2.5% HNTs; (d) 5% HNTs; (e) 7.5% HNTs; and (f) 10% HNTs.

Figure 3a,b shows the SEM morphologies of the surfaces of SPR chips before and after HNTs deposition, respectively. The surfaces are very uniform, as shown in Figure 3a, which indicates the success of attachment of the gold film to the surface of slides. Figure 3b suggests that the HNTs formed a compact but disordered rough surface on the gold film. As mentioned above, HNTs exhibit a high RI (1.550 RIU) compared to silica (1.458 RIU).[42,48] Therefore, strong evanescent light along the interface of the gold film can be easily coupled to the outer space. This further enhances the interaction of light and surrounding medium, which results in an enhanced sensitivity to the change of the external environment. In addition, the HNTs with a high aspect ratio of ~20 also contribute to the improvement of sensitivity.[49]

AFM was further used to characterize the surface morphology, thickness, and roughness of the attached HNTs on the HNTs-SPR sensor surface (Figure 4a). HNTs with a high aspect ratio can be identified from these $5 \times 5\ \mu m^2$ 3D images. It is observed that the coating surface is very rough and the morphology of disordered nanotubes close-packed on the substrate is consistent with the previous SEM results. The height profile in Figure 4b suggests that the thicknesses of all HNTs layers are in a normal distribution. The average thicknesses are 292.3, 344.0, 459.2, and 566.9 nm for 1, 2.5, 5, and 7.5% HNTs, respectively. Figure 4c suggests that there is a linear relationship between the HNTs concentration and the thickness of HNTs layers. This can be easily understood because the coating thickness is directly related to the amount of materials deposited on the substrates. Moreover, the root-mean-square roughness (R_q) for the HNTs coating, which takes the measures of the height of the surface profile $Z(x)$, shows a rising tendency when the HNTs concentration increases. The function R_q is described as follows:[50]

$$R_q = \sqrt{\frac{1}{L}\int_0^L |Z^2(x)|dx} \quad (1)$$

where $Z(x)$ is the function that describes the surface profile analyzed in terms of height (Z) and position (x) of the sample over the evaluation length L. Specifically, R_q of 1% HNTs is 83 nm, whereas it is 129 nm for 7.5% HNTs. The roughness of the HNTs coating is much higher than that of the previously reported HNTs coating (49 nm for 1% HNTs),[51] which can be explained by the different substrates and also by the different dispersion states in different dispersion media. It should be noted that R_q of the HNTs layers is not presenting a good linear relationship with HNTs concentration, especially at a relatively high HNTs concentration. This arises from the fact that R_q is related to the surface topography of the HNTs coating and depends on the swept area and the scan size of the sample. R_q is very sensitive to peaks and valleys, which are related to the arrangement and the aggregation state of the nanotubes on HNTs coating surfaces. This is most likely due to the merging of nanoparticles when a greater amount of materials were deposited on the surface. Actually, the increase of nanoparticle concentration induces the saturation of R_q, which is also found in other systems. We have also measured the AFM images of 10% HNTs coating. However, it was found that the nanotubes may be easily peeled off from the substrates because of the unduly thick layers of HNTs (estimated to be thicker than 650 nm) and the weak binding forces. Therefore, no high-resolution AFM images of 10% HNTs can be acquired.

HNTs-SPR Enhancement Efficiency. The performances of the five HNTs-SPR sensors are compared to that of a conventional (bare gold film) one. Figure 5 shows the transmittance spectra for the SPR sensors, with the RI of analytes changing from 1.333 to 1.355 RIU, which is within the RI range of biofluids. It is obvious that all transmittance spectra exhibit obvious SPR dips except for the sensor sprayed with 10% HNTs, and the dip red-shifts as the surrounding RI becomes higher. When the HNTs concentration increases, as shown in Figure 5a–e, the amount of the wavelength drift expands from 49.9 to 282.8 nm with the help of multiple advantages of HNTs; the average width of SPR dips obviously extends from 110.2 to 150.2 nm because of the strong scattering caused by the large amount of nanotubes on the gold film. However, the thickness of the HNTs layer for the 10% HNTs coating is estimated to be higher than 650 nm, which is too large for the evanescent light to interact with the analyte. Therefore, the sensor does not exhibit

DOI: 10.1021/acsami.7b16511
ACS Appl. Mater. Interfaces 2018, 10, 5933–5940

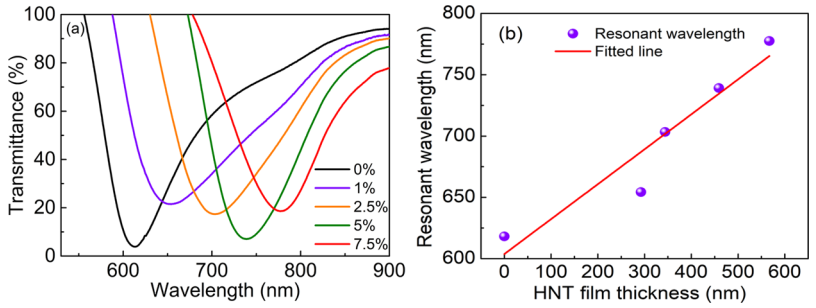

Figure 6. (a) Spectra of HNTs-SPR sensors for different concentrations at an environment RI of 1.333 RIU; (b) relationship between the resonance wavelength and the HNTs film thickness.

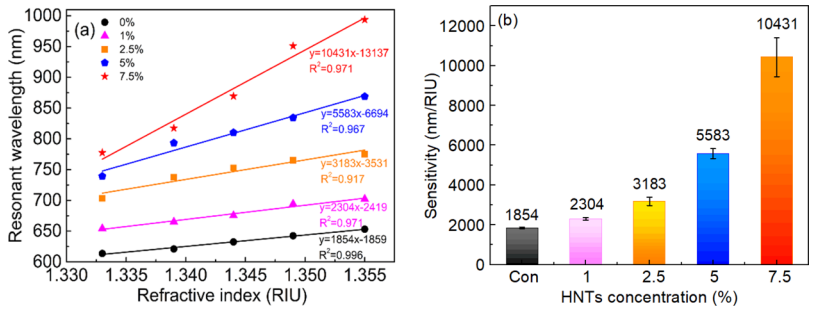

Figure 7. (a) Experimental variation of the resonance wavelength for the HNTs-SPR sensors with different concentrations; (b) sensitivity comparison for HNTs-SPR sensors coated with different HNTs concentrations.

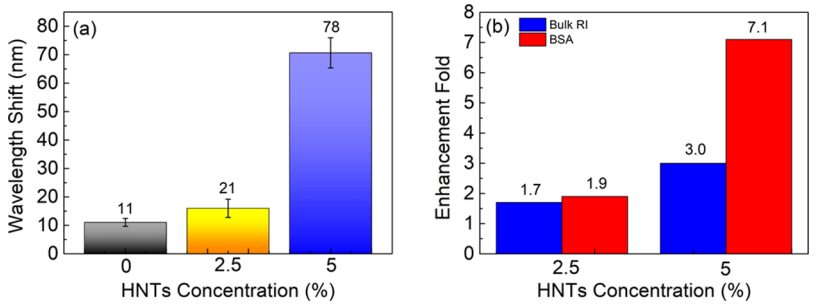

Figure 8. (a) Resonance wavelength shift for the control SPR sensor and HNTs-SPR sensors modified with different concentrations of HNTs, when flowed through phosphate buffer and BSA solutions (~1 mg/mL) successively. (b) Comparison of the sensitivity enhancement fold for the HNTs-SPR sensor when tested in bulk RI solutions and BSA solutions.

any sensitivity. The spectra for n_a = 1.333 RIU from 0−7.5% HNTs-SPR spectra were picked out and compared in Figure 6a. It is apparent that the resonance dips shift to a longer wavelength as the concentration of HNTs sprayed on the gold film at the same RI increases. Further analysis suggests a linear relationship between the resonance wavelength and the HNTs concentration, as shown in Figure 6b, which in turn corresponds to the thickness of the HNTs layer. The fitting function is $y = 0.28x + 603.7$, and the fitting coefficient R^2 is 0.88. According to this fitted line, one can also estimate the thickness of the attached HNTs layer with the resonant wavelength. The effective RI of the SPR sensor is boosted by the introduction of the HNTs layer.

Additionally, all resonance wavelengths in Figure 5a−e and their corresponding RIs were chosen for comparison in Figure 7a. It reveals that the resonance wavelengths for all thicknesses of the HNTs layers shift to longer wavelengths when the RI of the sensing medium increases. The sensitivity is the slope of the linear fitting of experimental data,[52] and the regression equations of the slope of each curve are 10 431 nm/RIU for 7.5% HNTs, 5583 nm/RIU for 5% HNTs, 3183 nm/RIU for 2.5% HNTs, 2034 nm/RIU for 1% HNTs, and 1854 nm/RIU for the conventional Au-film-based SPR chip. It is worth noting that the resonance wavelengths are in a good linear relationship with the HNTs concentration because all linearities are higher than 0.917. An increasing trend of the sensitivity of the HNTs-SPR sensor is shown in Figure 7b. The sensitivities of all HNTs-SPR sensors are all higher than that of the control one. Because the sensor modified with HNTs of 10% does not exhibit a useful resonance spectrum, it is concluded that the highest enhancement is 5.6-folds over the bare gold film chip, achieved at a concentration of 7.5% HNTs.

To further confirm the sensitivity enhancement of HNTs-SPR sensors in biological experiments, the phosphate buffer and BSA solutions (~1 mg/mL) were successively flowed through the HNTs-SPR sensors modified with HNTs solutions of 2.5, 5, and 7.5% and a control SPR sensor without HNTs modification was tested as well. The observed resonance wavelength shifts are 11, 21, and 78 nm for the control SPR and HNTs-SPR of 2.5 and 5%, respectively. Because the resonance wavelength for HNTs-SPR-7.5% in the BSA experiment falls in the range of 950−1000 nm,

DOI: 10.1021/acsami.7b16511
ACS Appl. Mater. Interfaces 2018, 10, 5933−5940

Table 1. Comparison of the Sensing Performance Enhanced by Various NanoMaterials

plasmonic interface	detection range (RIU)	sensitivity	enhanced fold	theoretical/experimental	references
Cu−TiO_2	1.33−1.37	∼3000 nm/RIU	∼2.5	experimental	15
Au−Si	1.33−1.358	4110 nm/RIU		experimental	14
Au−Si−WS_2	∼1.33	155.68 deg/RIU	∼3	theoretical	26
Au−Si−graphene			2	theoretical	29
Au−graphene	∼1.33		1.25	theoretical	28
Au−graphene	1.33−1.36	5400 nm/RIU		theoretical	24
Ag−graphene	1.33−1.37	91.76 au/RIU	1.22	theoretical	25
plasmonic nanorod metamaterial		30000 nm/RIU		experimental	20
Au−HNTs	1.333−1.355	10431 nm/RIU	5.6	experimental	this paper

the signal-to-noise ratio of the spectrometer is insufficient to record high-quality spectral data. Compared to the control sensor, the modification with HNTs solutions of 2.5 and 5% provides sensitivity enhancement by 1.9 and 7.1-folds, respectively. This result shows that the modification of SPR with HNTs could improve the sensitivity not only in the bulk solutions but also in the biomolecular experiments. It can be further found from Figure 8b that the enhancement folds achieved in the BSA solutions are even greater than those in pure RI solution under the same HNTs modification conditions. This is attributed to the fact that the HNTs layer has a larger surface area and accommodates much more BSA molecules than the gold film.

Comparison. To further verify the SPR enhancement efficiency from the HNTs, we summarize the comparison among different plasmonic interfaces in Table 1, in terms of the RI detection range of the analyte, sensitivity, enhancement fold, and the data acquisition approach. The RIs for all measurements are within 1.33−1.37 RIU in the published literature and the present work. Both conventional materials such as titanium dioxide and silicon and the new two-dimensional nanosheets such as WS_2 and graphene show lower SPR sensitivity and enhanced fold when compared to the present natural HNTs. Therefore, it is concluded that the HNTs-SPR sensor possesses significant superiority in terms of both sensitivity (10 431 nm/RIU) and enhancement (5.6-fold). The significant enhancement is attributed to the fact that HNTs simultaneously possess high RI, large surface area, and negatively charged surface. First, the HNTs layer possesses a relatively higher RI than the analyte solution,[42] which produces a stronger evanescent wave and thus results in a higher sensitivity.[23] Second, because of the electronegativity of the HNTs, a mass of electrons are transferred from the HNTs to the gold film surface, leading to a strong enhancement of the excited electric field in the sensing area. Furthermore, the hollow and curled nanostructure of the HNTs provides a better interaction between the sensing field and the detected substance. The overlap of the excited electric field of adjacent HNTs confines a strong plasmon-mediated energy inside the HNTs layer. The comprehensive effect of the three factors mentioned above has boosted the sensitivity of the HNTs-SPR sensor to a relatively higher level than those affected by any single factor. It is worth noting that the enhancing technique presented in this paper takes the SPR sensor into a new level of sensitivity with up to 10^4 nm/RIU in a wide RI range. This may enable SPR detection to break the limit of small molecules with a molecular weight less than 400 Da without any chemical or biological amplification1.[12]

CONCLUSIONS

We have proposed and demonstrated a novel technique to amplify the sensitivity of the SPR sensor by introducing natural HNTs to modify the surface of gold substrates. Benefiting from the excellent properties of the HNTs, such as a large surface area, high RI, and negatively charged surface, the firmly attached HNTs layer increases the intensity of the evanescent field and in turn improves the sensitivity of the SPR sensor. The sensitivity of the HNTs-SPR sensor increases with the HNTs concentration from 1 to 7.5%. The proposed sensors show significant superiority in terms of the highest sensitivity (10 431 nm/RIU) and the enhancement fold (5.6-folds) over those reported previously, for both conventional nanomaterial and two-dimensional material. Furthermore, all HNTs-SPR sensors exhibit good linearity (higher than 0.917) when the RI varies within the range of biofluids. Providing the many excellent interface properties of HNTs, the highly enhanced sensitivity of the HNTs-SPR sensors, and the simple process without chemical or biological amplification, the HNTs are expected to be a promising candidate material to address the current challenges of the SPR technique and act as a universal and highly sensitive platform for label-free analysis of small molecules and ultralow concentration of the analytes.

ASSOCIATED CONTENT

Supporting Information

The Supporting Information is available free of charge on the ACS Publications website at DOI: 10.1021/acsami.7b16511.

Experimental variation of shift in the resonance wavelength with RI and evanescent electric field distribution with different deposited layer thicknesses (PDF)

AUTHOR INFORMATION

Corresponding Authors

*E-mail: yunhanluo@163.com (Y.L.).
*E-mail: liumx@jnu.edu.cn (M.L.).

ORCID

Mei Yang: 0000-0003-0367-2841
Mingxian Liu: 0000-0002-5466-3024

Author Contributions

M.Y. and X.X. equally contributed to this work.

Notes

The authors declare no competing financial interest.

ACKNOWLEDGMENTS

This work was supported by the National Natural Science Foundation of China (nos. 61575084, 51502113, 61405075, 61475066, and 61505069), the National High Technology

DOI: 10.1021/acsami.7b16511
ACS Appl. Mater. Interfaces 2018, 10, 5933−5940

Research and Development Program of China (2015AA020915), the Natural Science Foundation of Guangdong Province (nos. 2015A030313320, 2015A030306046, 2016A030311019, 2016A030313079, and 2016A030310098), the Science and Technology Projects of Guangdong Province (nos. 2017A010101013, 2015B010125007, 2016B010111003, and 2016A010101017), and the Science & Technology Project of Guangzhou (nos. 201707010500, 201506010046, 201607010134, 201605030002, and 201610010026).

REFERENCES

(1) Homola, J.; Yee, S. S.; Gauglitz, G. Surface plasmon resonance sensors: review. *Sens. Actuators, B* **1999**, *54*, 3−15.
(2) Yuan, Y.; Ding, L.; Guo, Z. Numerical investigation for SPR-based optical fiber sensor. *Sens. Actuators, B* **2011**, *157*, 240−245.
(3) Iadicicco, A.; Cusano, A.; Cutolo, A.; Bernini, R.; Giordano, M. Thinned fiber Bragg gratings as high sensitivity refractive index sensor. *IEEE Photonics Technol. Lett.* **2004**, *16*, 1149−1151.
(4) Gao, Y.; Zou, F.; Wu, B.; Wang, X.; Zhang, J.; Koh, K.; Chen, H. CB[7]-mediated signal amplification approach for sensitive surface plasmon resonance spectroscopy. *Biosens. Bioelectron.* **2016**, *81*, 207−213.
(5) Lee, B.; Roh, S.; Park, J. Current status of micro- and nano-structured optical fiber sensors. *Opt. Fiber Technol.* **2009**, *15*, 209−221.
(6) Yang, M.; Long, S.; Zhu, W.; Luo, Y.; Mao, P.; Tang, J.; Fang, J.; Yu, J.; Zhang, J.; Lu, H.; Chen, Z. Design and optimization of nano-column array based surface plasmon resonance sensor. *Opt. Quantum Electron.* **2017**, *49*, 31.
(7) Ge, J.; Feng, H.; Chen, Y.; Tse, Z. T. H.; Fok, M. P. Spiral-structured fiber Bragg grating for contact force sensing through direct power measurement. *Opt. Express* **2014**, *22*, 10439−10445.
(8) Mao, P.; Luo, Y.; Chen, C.; Peng, S.; Feng, X.; Tang, J.; Fang, J.; Zhang, J.; Lu, H.; Yu, J.; Chen, Z. Design and optimization of surface plasmon resonance sensor based on multimode fiber. *Opt. Quantum Electron.* **2015**, *47*, 1495−1502.
(9) Karlsson, R.; Stahlberg, R. Surface plasmon resonance detection and multispot sensing for direct monitoring of interactions involving low-molecular-weight analytes and for determination of low affinities. *Anal. Biochem.* **1995**, *228*, 274−280.
(10) Gnedenko, O. V.; Mezentsev, Y. V.; Molnar, A. A.; Lisitsa, A. V.; Ivanov, A. S.; Archakov, A. I. Highly sensitive detection of human cardiac myoglobin using a reverse sandwich immunoassay with a gold nanoparticle-enhanced surface plasmon resonance biosensor. *Anal. Chim. Acta* **2013**, *759*, 105−109.
(11) Guo, L.; Jackman, J. A.; Yang, H.-H.; Chen, P.; Cho, N.-J.; Kim, D.-H. Strategies for enhancing the sensitivity of plasmonic nanosensors. *Nano Today* **2015**, *10*, 213−239.
(12) Zeng, S.; Baillargeat, D.; Ho, H.-P.; Yong, K.-T. Nanomaterials enhanced surface plasmon resonance for biological and chemical sensing applications. *Chem. Soc. Rev.* **2014**, *43*, 3426−3452.
(13) Mei, Q.; Ding, X.; Chen, Y.; Hong, J.; Koh, K.; Lee, J.; Chen, H.; Yin, Y. Comparative SPR study on the effect of nanomaterials on the biological activity of adsorbed proteins. *Microchim. Acta* **2012**, *178*, 301−307.
(14) Chen, H.; Hou, Y.; Ye, Z.; Wang, H.; Koh, K.; Shen, Z.; Shu, Y. Label-free surface plasmon resonance cytosensor for breast cancer cell detection based on nano-conjugation of monodisperse magnetic nanoparticle and folic acid. *Sens. Actuators, B* **2014**, *201*, 433−438.
(15) Lee, E. G.; Park, K. M.; Jeong, J. Y.; Lee, S. H.; Baek, J. E.; Lee, H. W.; Jung, J. K.; Chung, B. H. Carbon nanotube-assisted enhancement of surface plasmon resonance signal. *Anal. Biochem.* **2011**, *408*, 206−211.
(16) *Reviews in Plasmonics 2010*; Geddes, G. D., Ed.; Springer, 2012.
(17) Lin, Y.; Zou, Y.; Lindquist, R. G. A reflection-based localized surface plasmon resonance fiber-optic probe for biochemical sensing. *Biomed. Opt. Express* **2011**, *2*, 478−484.
(18) Jia, S.; Li, P.; Koh, K.; Chen, H. A cytosensor based on NiO nanoparticle-enhanced surface plasmon resonance for detection of the breast cancer cell line MCF-7. *Microchim. Acta* **2015**, *183*, 683−688.
(19) Kabashin, A. V.; Evans, P.; Pastkovsky, S.; Hendren, W.; Wurtz, G. A.; Atkinson, R.; Pollard, R.; Podolskiy, V. A.; Zayats, A. V. Plasmonic nanorod metamaterials for biosensing. *Nat. Mater.* **2009**, *8*, 867−871.
(20) Singh, S.; Gupta, B. D. Fabrication and characterization of a surface plasmon resonance based fiber optic sensor using gel entrapment technique for the detection of low glucose concentration. *Sens. Actuators, B* **2013**, *177*, 589−595.
(21) Coelho, L.; Viegas, D.; Santos, J. L.; de Almeida, J. M. M. M. Characterization of zinc oxide coated optical fiber long period gratings with improved refractive index sensing properties. *Sens. Actuators, B* **2016**, *223*, 45−51.
(22) Bhatia, P.; Gupta, B. D. Surface plasmon resonance based fiber optic refractive index sensor utilizing silicon layer: Effect of doping. *Opt. Commun.* **2013**, *286*, 171−175.
(23) Singh, S.; Mishra, S. K.; Gupta, B. D. Sensitivity enhancement of a surface plasmon resonance based fibre optic refractive index sensor utilizing an additional layer of oxides. *Sens. Actuators, A* **2013**, *193*, 136−140.
(24) Lee, K.-S.; El-Sayed, M. A. Gold and silver nanoparticles in sensing and imaging: sensitivity of plasmon response to size, shape, and metal composition. *J. Phys. Chem. B* **2006**, *110*, 19220−19225.
(25) Malinsky, M. D.; Kelly, K. L.; Schatz, G. C.; Van Duyne, R. P. Chain length dependence and sensing capabilities of the localized surface plasmon resonance of silver nanoparticles chemically modified with alkanethiol self-assembled monolayers. *J. Am. Chem. Soc.* **2001**, *123*, 1471−1482.
(26) Jain, P. K.; Huang, X.; El-Sayed, I. H.; El-Sayed, M. A. Review of Some Interesting Surface Plasmon Resonance-enhanced Properties of Noble Metal Nanoparticles and Their Applications to Biosystems. *Plasmonics* **2007**, *2*, 107−118.
(27) Law, W.-C.; Yong, K.-T.; Baev, A. Sensitivity improved surface plasmon resonance biosensor for cancer biomarker detection based on plasmonic enhancement. *ACS Nano* **2011**, *5*, 4858−4864.
(28) Wu, L.; Chu, H. S.; Koh, W. S.; Li, E. P. Highly sensitive graphene biosensors based on surface plasmon resonance. *Opt. Express* **2010**, *18*, 14395−14400.
(29) Verma, R.; Gupta, B. D.; Jha, R. Sensitivity enhancement of a surface plasmon resonance based biomolecules sensor using graphene and silicon layers. *Sens. Actuators, B* **2011**, *160*, 623−631.
(30) Feng, D.; Liu, G.; Zhang, M.; Jia, D. D-shaped fiber optic SPR biosensors based on a metal-graphene structure. *Chin. Opt. Lett.* **2013**, *11*, 110607−110610.
(31) Maharana, P. K.; Padhy, P.; Jha, R. On the field enhancement and performance of an ultra-stable SPR biosensor based on graphene. *IEEE Photonics Technol. Lett.* **2013**, *25*, 2156−2159.
(32) Ouyang, Q.; Zeng, S.; Jiang, L.; Hong, L.; Xu, G.; Dinh, X.-Q.; Qian, J.; He, S.; Qu, J.; Coquet, P.; Yong, K.-T. Sensitivity Enhancement of Transition Metal Dichalcogenides/Silicon Nanostructure-based Surface Plasmon Resonance Biosensor. *Sci. Rep.* **2016**, *6*, 28190.
(33) Szunerits, S.; Maalouli, N.; Wijaya, E.; Vilcot, J.-P.; Boukherroub, R. Recent advances in the development of graphene-based surface plasmon resonance (SPR) interfaces. *Anal. Bioanal. Chem.* **2013**, *405*, 1435−1443.
(34) Fakhrullina, G. I.; Akhatova, F. S.; Lvov, Y. M.; Fakhrullin, R. F. Toxicity of halloysite clay nanotubes in vivo: a Caenorhabditis elegans study. *Environ. Sci.: Nano* **2015**, *2*, 54−59.
(35) Massaro, M.; Riela, S.; Lo Meo, P.; Noto, R.; Cavallaro, G.; Milioto, S.; Lazzara, G. Functionalized halloysite multivalent glyco-cluster as a new drug delivery system. *J. Mater. Chem. B* **2014**, *2*, 7732−7738.
(36) Yang, J.; Wu, Y.; Shen, Y.; Zhou, C.; Li, Y.-F.; He, R.-R.; Liu, M. Enhanced Therapeutic Efficacy of Doxorubicin for Breast Cancer Using Chitosan Oligosaccharide-Modified Halloysite Nanotubes. *ACS Appl. Mater. Interfaces* **2016**, *8*, 26578−26590.
(37) Jana, S.; Kondakova, A. V.; Shevchenko, S. N.; Sheval, E. V.; Gonchar, K. A.; Timoshenko, V. Y.; Vasiliev, A. N. Halloysite nanotubes with immobilized silver nanoparticles for anti-bacterial application. *Colloids Surf., B* **2017**, *151*, 249−254.

DOI: 10.1021/acsami.7b16511
ACS Appl. Mater. Interfaces 2018, 10, 5933−5940

(38) Liu, M.; He, R.; Yang, J.; Zhao, W.; Zhou, C. Stripe-like Clay Nanotubes Patterns in Glass Capillary Tubes for Capture of Tumor Cells. *ACS Appl. Mater. Interfaces* **2016**, *8*, 7709−7719.
(39) Bertolino, V.; Cavallaro, G.; Lazzara, G.; Milioto, S.; Parisi, F. Biopolymers-targeted adsorption onto halloysite nanotubes in aqueous media. *Langmuir* **2017**, *33*, 3317−3323.
(40) Liu, M.; Huo, Z.; Liu, T.; Shen, Y.; He, R.; Zhou, C. Self-Assembling Halloysite Nanotubes into Concentric Ring Patterns in a Sphere-on-Flat Geometry. *Langmuir* **2017**, *33*, 3088−3098.
(41) Liu, M.; Zhang, Y.; Li, J.; Zhou, C. Chitin-natural clay nanotubes hybrid hydrogel. *Int. J. Biol. Macromol.* **2013**, *58*, 23−30.
(42) Liu, M.; Guo, B.; Du, M.; Jia, D. Drying induced aggregation of halloysite nanotubes in polyvinyl alcohol/halloysite nanotubes solution and its effect on properties of composite film. *Appl. Phys. A* **2007**, *88*, 391−395.
(43) Vergaro, V.; Abdullayev, E.; Lvov, Y. M.; Zeitoun, A.; Cingolani, R.; Rinaldi, R.; Leporatti, S. Cytocompatibility and uptake of halloysite clay nanotubes. *Biomacromolecules* **2010**, *11*, 820−826.
(44) Liu, M.; Shen, Y.; Ao, P.; Dai, L.; Liu, Z.; Zhou, C. The improvement of hemostatic and wound healing property of chitosan by halloysite nanotubes. *RSC Adv.* **2014**, *4*, 23540−23553.
(45) Mitchell, M. J.; Castellanos, C. A.; King, M. R. Surfactant functionalization induces robust, differential adhesion of tumor cells and blood cells to charged nanotube-coated biomaterials under flow. *Biomaterials* **2015**, *56*, 179−186.
(46) Zieba, M.; Hueso, J. L.; Arruebo, M.; Martínez, G.; Santamaría, J. Gold-coated halloysite nanotubes as tunable plasmonic platforms. *New J. Chem.* **2014**, *38*, 2037−2042.
(47) Rui, R.; Xiaolong, X.; Shanshan, Z.; Bing, L.; Xue, W.; Kaibin, T. Facile preparation of homogeneous and length controllable halloysite nanotubes by ultrasonic scission and uniform viscosity centrifugation. *Chem. Eng. J.* **2016**, *291*, 20−29.
(48) Tan, G. L.; Lemon, M. F.; Jones, D. J.; French, R. H. Optical properties and London dispersion interaction of amorphous and crystalline SiO_2 determined by vacuum ultraviolet spectroscopy and spectroscopic ellipsometry. *Phys. Rev. B: Condens. Matter Mater. Phys.* **2005**, *72*, 205117.
(49) Zhu, J.; Deng, X.-c. Improve the refractive index sensitivity of gold nanotube by reducing the restoring force of localized surface plasmon resonance. *Sens. Actuators, B* **2011**, *155*, 843−847.
(50) Gadelmawla, E. S.; Koura, M. M.; Maksoud, T. M. A.; Elewa, I. M.; Soliman, H. H. Roughness parameters. *J. Mater. Process. Technol.* **2002**, *123*, 133−145.
(51) He, R.; Liu, M.; Shen, Y.; Long, Z.; Zhou, C. Large-area assembly of halloysite nanotubes for enhancing the capture of tumor cells. *J. Mater. Chem. B* **2017**, *5*, 1712−1723.
(52) Chiu, N.-F.; Huang, T.-Y. Sensitivity and kinetic analysis of graphene oxide-based surface plasmon resonance biosensors. *Sens. Actuators, B* **2014**, *197*, 35−42.

DOI: 10.1021/acsami.7b16511
ACS Appl. Mater. Interfaces 2018, 10, 5933−5940